HHS Public Access

Author manuscript

Nat Biotechnol. Author manuscript; available in PMC 2017 August 06.

Published in final edited form as:

Nat Biotechnol. 2017 March ; 35(3): 264–272. doi:10.1038/nbt.3801.

Gene Therapy Restores Auditory and Vestibular Function in a Mouse Model of Usher Syndrome Type 1c

Bifeng Pan[1,*], **Charles Askew**[1,*], **Alice Galvin**[1,*], **Selena Heman-Ackah**[1], **Yukako Asai**[1], **Artur A. Indzhykulian**[2], **Francine M. Jodelka**[3], **Michelle L. Hastings**[3], **Jennifer J. Lentz**[4], **Luk H. Vandenberghe**[5], **Jeffrey R. Holt**[1,6], and **Gwenaëlle G.S. Géléoc**[1]

[1]Dpt of Otolaryngology, F.M. Kirby Center for Neurobiology, Boston Children's Hospital, Harvard Medical School, Boston, MA

[2]Dpt of Neurobiology, Harvard Medical School, Boston, MA

[3]Dpt of Cell Biology & Anatomy, Chicago Medical School, Rosalind Franklin University of Medicine and Science, Chicago, IL

[4]Dpt of Otorhinolaryngology & Bio-communications and Neuroscience Center, LSU Health Sciences Center, New Orleans, LA

[5]Schepens Eye Research Institute, Boston, MA

[6]Dpt of Neurology, F.M. Kirby Center for Neurobiology, Boston Children's Hospital, Harvard Medical School, Boston, MA

Abstract

Because there are currently no biological treatments for deafness, we sought to advance gene therapy approaches to treat genetic deafness. We reasoned that gene delivery systems that target auditory and vestibular sensory cells with high efficiency would be required to restore complex auditory and balance function. We focused on Usher Syndrome, a devastating genetic disorder that

Correspondence should be addressed to G.S.G. (Gwenaelle.Geleoc@Childrens.harvard.edu).

*These authors contributed equally

Present addresses:

C. Askew: Gene Therapy Center, University of North Carolina, Chapel Hill, NC.

S. Heman-Ackah: MedStar Washington Hospital Center, Georgetown University Medical Center, Washington, DC

Authors Contributions

The project was conceived by G.S.G. Experiments were designed by G.S.G.

C.A performed RWM injections with AAV2/1 vectors, electrophysiological recordings and analysis of OHCs, FM1-43 imaging of the organ of Corti; B.P. carried out RWM injections with AAV/Anc80L65 vectors, electrophysiological recordings and analysis of IHCs mechanotransduction currents. G.S.G. performed electrophysiological recordings of vestibular hair cells. A.G., S.H.A. and G.S.G. performed auditory brainstem responses experiments. Semi-quantitative radiolabeled PCR and RT-PCR was performed by F.M.J. and M.L.H. ABR and behavioral data analysis was performed by A.G. and G.S.G. Y.A designed and prepared the plasmid constructs. SEM was performed by J.J.L. (P18), and A.I. (P8 and 6 weeks). DIC, immunostaining and confocal imaging was performed by G.S.G. L.H.V. assisted with production of AAV vectors. J.R.H assisted with the design of the experiments, preparation of figures and manuscript. G.S.G. analyzed, interpreted the results and wrote the manuscript.

Competing Financial Interests Statement

A patent #00633-0203P01 on "Materials and methods for delivering nucleic acids to cochlear and vestibular cells" has been deposited by L.H.V., G.S.G. & J.R.H. The Anc80L65 vector is patented by L.H.V., patent #WO/2015/054653 – "Methods of predicting ancestral virus sequence and uses thereof. L.H.V. is co-founder and SAB member of GenSight Biologics and consultant to various gene therapy companies. LHV receives research support from Selecta Biosciences and Lonza Houston on Anc-AAV development and discovery.

causes blindness, balance disorders and profound deafness, and used a knock-in mouse model, *Ush1c c.216G>A,* which carries a cryptic splice site mutation found in French-Acadian patients with Usher Syndrome type IC (USH1C). Following delivery of wild-type *Ush1c* into the inner ears of neonatal *Ush1c c.216G>A* mice, we find recovery of gene and protein expression, restoration of sensory cell function, rescue of complex auditory function and recovery of hearing and balance behavior to near wild-type levels. The data represent unprecedented recovery of inner ear function and suggest that biological therapies to treat deafness may be suitable for translation to humans with genetic inner ear disorders.

Introduction

Hearing loss affects ~250 million people worldwide, with an estimated half of those cases being due to inherited genetic mutations. Recent success using gene therapy in the inner ears of animal models provides proof-of-principal that the approach may be used to restore function for genetic deafness in humans. However, progress thus far has been limited and has failed to restore the exquisite sensitivity of the healthy mammalian inner ear. A significant short coming has been the lack of efficient vectors that target large numbers of sensory hair cells in the inner ear. For example, AAV2/8 vectors that encoded wild-type whirlin lead to rescue of inner hair cell (IHC) morphology but not outer hair cells (OHCs) or hearing function[1]. IHCs comprise about 25% of total auditory hair cells. The other 75% are OHCs, which are required to enhance the sensitivity and frequency selectivity of the inner ear. In another study, AAV2/1 vectors injected in *Tmc1* mutant mice, targeted 80–90% of IHCs and revealed moderate auditory rescue with minimal ABR thresholds of ~80 dB (8 kHz)[2]. Using a similar viral capsid and promoter that drove expression in just IHCs, yielded partial recovery of auditory function (thresholds ~60 dB at 8 kHz) in mice that lacked the IHC gene *Vglut3*[3]. While these studies have demonstrated exogenous gene delivery into auditory IHCs, gene delivery to OHCs has remained a challenge. Because many genes that cause deafness are expressed in both IHCs and OHCs, gene delivery methods that target both cell types are needed to restore complex auditory function. Among the genes expressed in both cell types are those that encode Usher Syndrome proteins.

Usher syndrome (USH) is a rare genetic condition that affects 16,000 to 20,000 people in the United States and is responsible for 3 to 6% of early childhood deafness[4,5,6]. Of three subtypes, Usher type I (USH1) is the most severe form. USH1 patients suffer profound sensorineural hearing loss, vestibular areflexia and progressive blindness. Unless fitted with a cochlear implant, USH1 patients do not recover auditory function or develop the ability to generate speech. Six genes are associated with USH1: *MYO7A* (myosin 7a)[7,8,9,10], *USH1C* (harmonin)[11,12], *CDH23* (cadherin 23)[13,14], *PCDH15* (protocadherin 15)[15,16,17], *SANS* (sans)[18] and *CIB2* (calcium and integrin binding protein 2)[19]. USH1 proteins are involved in morphogenesis of sensory hair bundles and are localized to the apex of hair cells in mechanosenosory hair bundles. Harmonin resides at the core of an USH1 interactome where it binds to other USH1 proteins. The *USH1C* gene includes 28 exons, which code for 10 alternative splice forms[11,12], grouped in three different subclasses (a, b and c) depending on the domain composition of the protein. In hair cells, harmonin is expressed during early postnatal stages but expression declines around postnatal day 30 (P30). The harmonin-b

splice form is found at the tips of stereocilia near the tip-link insertion point in mouse hair cells[20,21,22] where it plays a structural role and is likely required for sensory transduction in both auditory and vestibular hair cells [20,23]. Harmonin-a is localized at the synapse where it associates with $Ca_v1.3$ Ca^{2+} channels and limits channel availability through an ubiquitin-dependent pathway[24,25].

Of several mouse models for Usher syndrome characterized over the past decade, only one, *Ush1c c.216G>A*, reproduces both auditory and retinal deficits that typify human Usher I Syndrome. The *Ush1c c.216G>A* mutation affects expression of all conventional harmonin isoforms due to a point mutation similar to one found in a cohort of French-Acadian USH1C patients[26]. The mutation introduces a cryptic splice site at the end of exon three in the *Ush1c* gene and results in translation of a severely truncated protein[27]. Homozygous *Ush1c c.216G>A* mice (c.216AA) suffer from severe hearing loss at one month of age [28], while heterozygous c.216GA mice do not present any abnormal phenotype. Cochlear histology in c.216AA mice reveals disorganized hair bundles and loss of both inner and outer hair cells in middle and basal turns at P30[28].

To identify a therapeutic window for treatment, we studied the function and maintenance of hair cells in newborn c.216AA mice. Our data show that a large majority of c.216AA hair cells survive and remain mechanosensitive during the first postnatal week. Since reduced expression of full-length harmonin is the most likely cause of deafness in *USH1C c.216G>A* patients[27], we investigated whether early re-introduction of full-length harmonin in c.216AA hair cells would preserve hair cell and auditory function in homozygous c.216AA mice. We found that a synthetic adeno associated viral vectors (Anc80L65)[29] encoding harmonin-a or -b successfully transduced larger numbers IHCs and OHCs and drove harmonin expression and correct protein localization. Early postnatal round window membrane injection of harmonin vectors successfully restored auditory and vestibular function to near wild-type levels in otherwise deaf and dizzy c.216AA mice. Our results demonstrate that early re-introduction of wild-type harmonin with vectors that efficiently target inner and outer hair cells can improve auditory sensitivity by over a thousand-fold, relative to first generation inner ear gene therapy approaches.

Results

Hair cell survival in Ush1c mice

Homozygous c.216AA mice are deaf and show circling and head tossing behaviors characteristic of vestibular dysfunction[28]. At 1 month of age, there is pronounced inner and outer hair cell degeneration at the base of the cochlea and degeneration and hair cell death in the middle turn, while the apical portion of the organ is better preserved[28]. To assess hair cell survival at earlier stages, we performed scanning electron microscopy (SEM) analysis along the organ of Corti at P8 and P18. Outer hair cells (OHCs) and inner hair cells (IHCs) of heterozygous c.216GA mice were preserved and their bundles were properly oriented (Fig. 1a–c, g, i and Supplementary Fig. 1a–c, k). However, disorganized hair bundles were evident along the entire length of the organ of Corti in homozygous c.216AA mice at both ages analyzed (Fig. 1d–f, h, j–l and Supplementary Fig. 1d–j, l). At P8, IHC bundles were mildly disorganized at the base, mid and apical regions (Fig. 1d–f, j). While many OHCs of

c.216AA mice possessed well-preserved hair bundles (Fig. 1h, k), fragmented and disorganized hair bundles were evident sporadically along the organ (Fig. 1d–f, l). Disruption was more pronounced at P18, although the majority of hair cells were still present as previously reported[30] (Supplementary Fig. 1d–f).

To assess hair cell function at early stages, we analyzed uptake of FM1-43, a compound that permeates functional mechanosensitive channels[31,32,33], in inner ear organs at P4. Uniform FM1-43 uptake was observed in hair cells of c.216GA mice (Fig. 2a), but uptake varied among OHCs of c.216AA mice, suggesting that some, but not all, cells retained functional channels (Fig. 2b). FM1-43 uptake decreased in IHCs of c.216AA mice during the first postnatal week (not shown). In utricle hair cells of c.216AA mice, uptake was restricted to the extra-striola region at P6, suggesting that hair cells of the striola region lacked mechanosensitive channels open at rest (Fig. 2c, d).

Sensory transduction in Ush1c hair cells

Next, we assessed mechanotransduction currents in IHCs, OHCs and vestibular hair cells (VHCs) of c.216GA and c.216AA mice during the first postnatal week. Mechanotransduction currents were recorded in whole-cell voltage-clamp configuration in response to mechanical displacements of hair bundles by a stiff glass probes. In c.216AA mice, recordings were obtained from the middle and apical turns of the cochlea from P3 to P6. OHCs retained mechanosensitivity, although the amplitudes of the responses were reduced by ~63% to 170 ± 80 pA (n=24; $p<0.001$, Fig. 2e–g). Severely disorganized bundles had smaller currents than better preserved hair bundles (120 ± 65 pA, n=9 and 201 ± 74 pA, n=15, respectively). Despite the reduction in current amplitude, c.216AA OHC sensitivity to mechanical displacements was similar to that of heterozygous c.216GA hair cells (Fig. 2f, Supplementary Fig. 2b).

Similarly, while hair bundles from IHCs of c.216AA mice appeared only mildly disrupted under the DIC microscope, transduction currents were significantly reduced at P6 (Fig. 2e–g). Maximum transduction currents in heterozygous c.216GA IHCs (P6-P7) averaged 587 ± 96 pA (n=21) but were reduced by 46% to 316 ± 127 pA (n=19; $p<0.001$) in c.216AA IHCs. c.216AA IHCs showed a significant ($p<0.01$) reduction in sensitivity (Supplementary Fig. 2g). Adaptation, or the decline in transduction current in the presence of constant bundle deflection, was also present, but the rate and extent of adaptation was reduced in c. 216AA hair cells relatively c.216GA cells (Supplementary Fig. 2c–e, h–j). These results demonstrate that mechanosensitivity is mildly compromised in inner and outer hair cells of c.216AA mice and, importantly, that both cell types survive throughout the first postnatal week, a prerequisite for gene therapy and restoration of cellular function.

Vestibular hair cells of c.216AA mice also showed a reduction in mechanotransduction currents. In the extra-striola region, currents were significantly ($p<0.001$) reduced to 109 ± 30 pA (n=9, P5-P7) versus 231 ± 53 pA (n=8, P6-P7) for c.216GA currents (Fig. 2e, f, h). Very small or no currents were evoked from hair cells of the striola region (6 ± 13 pA, n=6, P5-P7), in agreement with the absence of FM1-43 uptake in that region (Fig. 2c,d). In conclusion, while utricle hair bundles appeared grossly well-preserved, transduction currents were significantly reduced in the extra-striola and absent in the striola.

Exogenous harmonin rescues sensory transduction in Ush1c hair cells

To assess whether AAV vectors can drive expression of exogenous harmonin splice forms, we exposed P1 utricles and organs of Corti from neonatal c.216AA, c.216GA and wild-type (C57BL/6J) mice to AAV2/1 vectors encoding EGFP fused to the N-terminus of harmonin-b1 (EGFP::harmonin-b1) or tdTomato fused to the N-terminus of harmonin-a1 (tdTomato::harmonin-a1). Hair cells of wild-type, c.216GA and c.216AA mice were successfully transduced *in vitro* (Fig. 3a–c, e). EGFP::harmonin-b1 signal was evident at the tips of the stereocilia in VHCs (Fig. 3a), IHCs and OHCs (Fig. 3b, c). EGFP signal was also detected at P60 in OHCs and IHCs in the basal portion of the cochlea of mice injected at P1 (Fig. 3d). TdTomato::harmonin-a1 was detected at the base of auditory hair cells (Fig. 3e). Co-staining with a ribbon synapse marker CTBP2 frequently revealed colocalization in P7 IHCs (Fig. 3e) but not in P7 utricles (data not shown). Localization of our exogenous fusion constructs was consistent with previous work that localized harmonin-b to the distal end of stereocilia, near the tip-link insertions[20,21,22], and harmonin-a to the synapse[24,25].

Next, we assessed function in c.216AA hair cells exposed to AAV vectors driving harmonin expression.

To enhance the likelihood of functional rescue, we packaged untagged harmonin-a1 or harmonin-b1 coding sequences driven by a CMV promoter into AAV2/Anc80L65[34]. We performed RWM injections at P1 of AAV2/Anc80L65.CMV.harmonin-b1 and separately a mixture of AAV2/Anc80L65.CMV.harmonin-a1 + AAV2/Anc80L65.CMV.harmonin-b1 and assessed mechanotransduction responses 2 weeks after treatment. Although mature OHCs (>P10) do not survive *ex-vivo* recording experiments, robust electrophysiological recordings were obtained from IHCs at the equivalent of P14-P16 (Fig. 4). While IHCs from uninjected mice displayed severely reduced transduction currents at P16 (79 ± 43 pA, n=8), significant recovery (***P<0.001) was observed in mice injected at P1 with harmonin-b1 or a combination of harmonin b1 and a1, with respective average maximal transduction currents of 388 ± 66 pA (n=15) and 352 ± 28 pA (n=7; Fig. 4c). Transduction current amplitudes in IHCs after treatment with harmonin-b1 or the combination of harmonin b1 and a1 were not significantly different from those of control c.216GA mice. These results suggest that delivery of exogenous harmonin-b1 via RWM injection at early stages can restore mechanotransduction in IHCs.

Rescue of auditory brainstem responses in Ush1c mice

To investigate rescue of auditory and balance function in *Ush1c* mice, we performed P0-P1 RWM injections of AAV2/Anc80L65.CMV.harmonin-a1 and/or AAV2/Anc80L65.CMV.harmonin-b1 and later assessed auditory brainstem responses (ABRs), distortion product otoacoustic emissions (DPOAEs), acoustic startle reflexes, open field and rotarod behavior. Mice were assessed at six weeks, a stage at which c.216AA mice show profound hearing loss and vestibular dysfunction. Some of the mice were further tested at 3 and 6 months. None of the 12 mice injected with AAV2/Anc80L65.CMV.harmonin-a1 recovered auditory function at 6 weeks (Fig. 5a–c), suggesting exogenous expression of harmonin-a1 was insufficient for auditory rescue. However, 19 of 25 mice injected with AAV2/Anc80L65.CMV.harmonin-b1 recovered significant auditory function (ABR

thresholds < 80 dB) at 6 weeks. The reason for lack of rescue in six of 25 mice was not clear, but may have been due to failed injections, clogged injection pipettes or injections that missed the targeted perilymphatic space. At low frequencies (5.6 to 16 kHz), the lowest ABR thresholds in AAV2/Anc80L65.CMV.harmonin-b1 injected ears were 25–30 dB, remarkably similar to thresholds of wild-type mice (Fig. 5a–b). Partial rescue was observed at 22.6 kHz and little to none at 32 kHz. Rescue of DPOAE thresholds was also evident (Fig. 5c) at low frequencies, consistent with rescue of OHC function. Eight of the mice that possessed auditory thresholds <45 dB for stimuli 8–11.3 kHz were tested at later stages to assess the longevity of the rescue. From 6 weeks to 3 months, ~10 dB ABR threshold shifts were observed in the low frequency range and ~30 dB in the high frequency range (Fig. 5d). A similar shift was also observed in the DPOAEs thresholds (Fig. 5e). After this time point, ABR and DPOAE thresholds remained stable up to 6 months (Fig. 5d–e), the latest time point tested.

To assess whether both harmonin-a1 and harmonin-b1 are required for more complete auditory rescue, particularly at the high frequency end, we co-injected two vectors, each driving expression of one splice form of harmonin. To confirm that both were targeted to the hair cells, AAV2/Anc80L65.CMV.tdTomato::harmonin-a1 and AAV2/Anc80L65.CMV.EGFP::harmonin-b1 were co-injected at P0-P1 (0.5μl + 0.5 μl). 65% of the hair cells expressed both harmonin-a1 and harmonin-b1, as evident from cells positive for both fluorescent tags (Supplementary Fig. 3). Fluorescently labeled harmonin-a1 was occasionally observed in the stereocilia of mice exposed to AAV2/Anc80L65.CMV.tdTomato::harmonin-a1, perhaps due to over expression. ABR and DPOAE thresholds in mice co-injected with unlabeled harmonin-a1 and harmonin-b1 vectors (Fig. 5) were similar to those of mice injected with harmonin-b1 alone, suggesting that harmonin-a1 may be dispensable for auditory function. Notably, harmonin-b1 alone was sufficient for significant restoration of auditory thresholds at low frequencies (Fig. 5).

To further characterize the rescue, ABR waveforms from mice with thresholds ≤45 dB were analyzed and compared between eight control c.216GA mice and five c.216AA mice injected with AAV2/Anc80L65.CMV.harmonin-b1. The analysis of waveform at 8, 11.3 and 16 kHz revealed normal wave 1 amplitudes, relative (non-significant differences, $P>0.2$, Student t-test) and longer peak 1 latencies ($P>0.001$) (Supplementary Fig. 4), suggesting a possible lag in neurotransmission at the synapse.

In many animals, auditory rescue was also observed in the contralateral ear, with ABR thresholds as low as 20 dB at 11.3 kHz (harmonin-b1: average 59.7 ± 5.3 dB, n=15/25; harmonin-a1+-b1: average 76.2 ± 10.3 dB, n=4/6). Diffusion of AAV vectors to the contralateral ear has been previously observed[35] and likely occurs via the cochlear aqueduct.

To determine whether injections at a later developmental stage might lead to partial auditory rescue, we performed RWM injections of AAV2/Anc80L65.CMV.harmonin-b1 (0.8 μl) at P10-P12 and assessed auditory thresholds at 6 weeks. None of these mice had detectable DPOAEs, and their ABR thresholds did not differ from the uninjected c.216AA control mice (n=10; data not shown).

To address the concern that truncated harmonin, a consequence of the *c.216G>A* mutation, may disrupt function by competing with full-length harmonin for endogenous binding partners[28,30], we generated Anc80L65.CMV.trunc-harm vectors that over-expressed the truncated protein and injected them via RWM into the inner ears of c.216GA mice. ABR and DPOAES measurements at 4, 6 and 12 weeks revealed no difference in thresholds between injected and uninjected c.216GA mice over the entire frequency range (Fig. 5b–c). These data, which also serve as a control for the injection technique and the vector, suggest that exogenous truncated harmonin does not compete with endogenous full-length harmonin.

Rescue of auditory and vestibular behavior in Ush1c mice

To assess whether the ABR/DPOAE recovery yielded behaviorally relevant recovery of auditory function, we measured acoustic startle responses in subsets of mice injected with AAV2/Anc80L65.CMV.harmonin-a1, AAV2/Anc80L65.CMV.harmonin-b1, or both vectors. Startle response to white noise showed partial rescue in 6 week old mice injected with AAV2/Anc80L65.CMV.harmonin-b1 and in mice co-injected with both vectors (Fig. 6a). Mice that received harmonin-a1 alone were similar to uninjected c.216AA mice and did not recover startle responses.

Since the perilymphatic space is continuous between the cochlea and vestibular labyrinth, AAV vectors injected via RWM may transduce vestibular sensory organs. To assess vestibular behavior, we tested performance of subsets of mice on a rotarod over five trials. While poor rotarod performance was observed in c.216AA and c.216AA mice injected with AAV2/Anc80L65.CMV.harmonin-a1 (latency to fall <22 sec on average), c.216AA mice injected with AAV2/Anc80L65.CMV.harmonin-b1 and those co-injected with harmonin-a1 and -b1 vectors maintained balance function on the rotarod for 60–120 seconds, consistent with control c.216GA mice (Fig. 6b). We also observed mice in a 42 cm wide open-field chamber for 5 min. Recovery in open-field behavior was evident in harmonin-b1 and dual harmonin-a1 and b1 injected c.216AA mice. Representative open-field exploration traces are plotted in Fig. 6c. c.216GA mice explored the border of the field and displayed minimal full-body rotations, whereas c.216AA mice displayed more activity throughout the entire chamber with increased full-body rotations quantified as rotations/min (Fig. 6d–e). Surprisingly, while no ABR rescue was observed in mice injected with AAV2/Anc80L65.CMV.harmonin-a1, open field data demonstrated recovery of normal behavior to the level of the control mice.

Hair bundle morphology in rescued Ush1c mice

We assessed hair bundle morphology with SEM in 6-week old mice that displayed rescue of auditory function. c.216AA mice displayed severe hair cells loss at the basal and middle regions of the organ (Fig. 7e–f). In the basal region, OHCs were mostly absent in the first row and present sporadically in the second and third rows. In the middle region of the organ, the first row of OHCs was also largely absent. Milder phenotypes were observed in the apical end. High magnification SEM also revealed severely disorganized hair bundles along the entire length of the organ of c.216AA mice. Notably, in 6-week old c.216AA mice, no hair bundles were observed that retained the typical staircase structure with all three rows of stereocilia (Fig. 7h). Instead hair bundles were disorganized, with retracted stereocilia along

the first row, abnormal second row and fairly preserved tallest row. In contrast, reduced hair cell loss and normal hair bundle morphologies were observed in c.216AA mice that showed recovery of function after treatment with harmonin-b1 (Fig. 7i–l, n–p). Hair cells counts were estimated from the presence or absence of hair bundles in representative fields of view. The data revealed pronounced preservation of hair cell numbers in injected mice from the base to the apex of the organ, from 40 to 79% in the base, 68 to 95% in the middle and 93 to 99% in the apex (n=1824 cells from n=4 c.216AA mice and n=792 from n=2 rescued c.216AA ears) (Fig. 7m). Although abnormal hair bundles were still evident in harmonin-b1 injected mice, most hair bundles possessed three rows of stereocilia and had morphology almost indistinguishable from that of their heterozygous controls (Fig. 7i, n, p).

Harmonin expression correlates with hair cell survival and ABR thresholds

To confirm expression of AAV2/Anc80L65.CMV.harmonin-b1 and explore the relationship between viral expression level and ABR thresholds, we quantified DNA and RNA isolated from individual injected and contralateral cochleas. Expression was assessed in six-week old c.216GA and AAV2/Anc80L65.CMV.harmonin-b1 injected and non-injected c.216AA mice. Mouse *Ush1c* RNA expressed from the AAV1/Anc80L65.CMV.harmonin-b1 vector (Supplementary Fig. 5a) and AAV2/Anc80L65.CMV.harmonin-b1 DNA (Supplementary Fig. 5b) were detected in all of the injected cochleas and, to a lesser extent, in the contralateral cochleas of injected animals. There was variability between animals in ABR thresholds and amount of DNA and RNA expressed (Supplementary Fig. 5c). However, we found a strong correlation between AAV2/Anc80L65.CMV.harmonin-b1 DNA levels, the amount of mRNA encoding the correctly spliced form of harmonin and ABR threshold levels, which suggests that the variability in ABR data may be a direct result of AAV expression. Absent or poor AAV expression levels likely resulted from failed RWM injections. To confirm that harmonin was expressed in rescued ears, we performed harmonin immunostaining in rescued cochleas as well as cochleas harvested from wild type, c.216AA and c.216AA mice with failed rescued. Specific harmonin labeling was observed at stereocilia tips in wild type and rescued ears but was absent in uninjected c.216AA ears and injected but not rescued c.216AA ears (Supplementary Fig. 5d).

To assess long-term hair cell survival in mice that had successful recovery of ABR thresholds, we prepared tissue and counted the number of IHCs and OHCs at 6 months of age from 5 mice (Supplementary Fig. 6). While the number of IHCs did not vary in the two cohorts, 50% or more OHCs remained in the three mice that showed long term ABR rescue. OHC survival was observed along the entire organ with the exception of the basal turn (Supplementary Fig. 6).

Discussion

While previous work has shown that homozygous knock-in c.216AA mice have significant hair cell degeneration at P18 and P30[27,28], in early postnatal c.216AA mice, we found altered hair bundle morphology, yet functionally viable hair cells, revealing a potential therapeutic window. During the first postnatal week, auditory and vestibular epithelia retained mechanosensitive hair cells, including some with relatively normal morphology

(Fig. 1). Transduction currents were diminished in amplitude but many auditory hair cells retained characteristics within the normal range for adaptation and sensitivity (Supplementary Fig. 2). In the vestibular system, c.216AA hair cells in the extra-striola region had reduced current amplitudes, whereas cells in the striola region did not take up FM1-43 and did not respond to bundle displacements (Fig. 2). Therefore, with the exception of the striola region, our results suggest that the transduction apparatus can be correctly assembled and targeted in mutant mice but that the number of functional complexes appears to be reduced during the neonatal period. Since a small percentage of correct splicing still occurs in c.216AA mice[30], we hypothesize that even low expression levels of wild-type harmonin may be sufficient for partial development and short-term maintenance of the transduction apparatus in homozygous c.216AA mice during early postnatal stages, allowing for an expanded therapeutic window. In contrast, previous work has shown that full knockouts of *Ush1c* have transduction currents that were nearly absent by P7[23] which we predict would limit the window for intervention.

We showed that AAV2/1 vectors successfully targeted hair cells and that harmonin fusion constructs were correctly localized (Fig. 3). EGFP::harmonin-b1 was targeted to the tips of stereocilia when transfected with AAV vectors in wild-type or mutant auditory or vestibular tissues, consistent with prior localization studies[23]. The harmonin-a1 variant is localized near the ribbon synapse where it interacts with CaV1.3 channels to alter exocytosis[24,25]. While expression of tdTomato::harmonin-a1 packaged in AAV2/1 was observed at the base of the IHCs and was absent from stereocilia, higher expression levels obtained with AAV2/Anc80L65 led to diffuse localization throughout the cell and in the stereociliary bundle. TdTomato::harmonin-a1 was also observed throughout the utricle, excluded from stereocilia and showed little colocalization with ribbon synapse markers at P7. While this may be a consequence of the tagged fluorescent marker, it is also possible that harmonin-a1 plays a different role in the utricle or that localization differs in more mature epithelia.

We studied whether expression of multiple harmonin isoforms are needed for full functional rescue in auditory and vestibular organs. Since harmonin-b plays an important role in the stereocilia and harmonin-a has been shown to alter exocytosis, we suspected that both splice forms would be necessary to rescue inner ear function. However, co-injection of harmonin-b1 and harmonin-a1 did not enhance recovery. Thus, harmonin-b1 alone was sufficient to restore partial function. ABR responses in rescued mice showed normal wave 1 amplitudes and longer peak 1 latencies relative to normal hearing controls (Supplementary Fig. 4), the latter perhaps due to an incomplete functional recovery at the synapse.

Auditory rescue was prominent at low but not high frequencies (Fig. 5), while hair bundles with normal morphology were observed along the entire organ at 6 weeks of age (Fig. 7). The absence of rescue at high frequencies is unlikely to have been caused by damage from the injection as high-frequency hearing loss was not observed in any injected c.216GA mice (Fig. 5b–c). Poor transduction efficiency at the base[26] is also an unlikely explanation given AAV targeting along the entire length of the cochlea[29]. It is possible that other harmonin isoforms, such as harmonin-c, may be necessary for rescue of function in the basal high frequency end of the cochlea. Alternatively, since cochlear development begins at the basal

end, by P0 these hair cells may have matured beyond the point of repair. If so, embryonic intervention[36,37] may be more effective.

In behavioral assays, harmonin-a1 mediated partial vestibular rescue (indicated by reduced circling behavior), whereas harmonin-b1 enabled more complete functional recovery in both vestibular tests (reduced circling and enhanced rotarod performance; Fig. 6). The absence of transduction and FM1-43 uptake in the striola regions argues that hair cells of the striola region and perhaps type I cell function depend on proper harmonin expression (Fig. 2). Further studies are needed to clarify the role of harmonin in the vestibular system. Additional assays of vestibular function, such as vestibular evoked potentials, may provide a physiological measure of the extent of rescue.

A previous study[30] restored function in early postnatal *Ush1c* mice using intra-peritoneal injection of antisense oligonucleotides targeting c.216AA. Another report corrected *Ush1c* gene expression in mice with the same antisense oligonucleotide delivered to the amniotic cavity[38]. An advantage of the antisense approach is that all splice forms may be expressed, however repeated injections may be needed to maintain long-term rescue. AAV vectors, on the other hand, can provide long-term transgene expression in post-mitotic tissue even in the absence of genome integration[39,40]. Our results obtained at 12 and 24 weeks suggest that this may indeed be the case in inner ear hair cells. Both strategies have now provided compelling evidence that gene therapy can be further developed to treat Usher Syndrome type 1C for patients who have the 216G>A splice site mutation and possibly other *USH1C* mutations.

In summary, our data provide further support for development of viral-mediated gene transfer in the inner ear to treat disorders that affect sensory hair cells. Here, using a vector with high transduction efficiency in both IHCs and OHCs, we show the most complete rescue of auditory function for any inner ear gene therapy application to date with over a thousand-fold improvement in sound pressure level sensitivity (thresholds ~25 dB at 8 kHz), relative to prior studies[2,3]. Furthermore, we show the most complete gene therapy recovery of vestibular function in a genetic model of combined auditory and vestibular dysfunction. Translation of these successes to the clinic will likely necessitate optimization of the delivery vectors, promoters and coding sequences, validation of the viral targeting and efficacy in larger animal models *in vivo*, and perhaps in human tissue *in vitro*, as well as a better understanding of the therapeutic window in humans. Lastly, while conventional AAV vectors have a good safety profile, next generation AAVs, such as Anc80L65, have not yet been evaluated in humans and thus will require careful scrutiny before wide-spread application.

Online Methods

Animals

Ush1c c.216G>A knock-in mice were obtained from Louisiana State University Health Science Center. The imported strain while on a C57BL6 background were previously bred out of the Cdh23 (Ahl) mutation causing age related hearing loss[41,42]. All procedures used for this work met the NIH guidelines for the care and use of laboratory animals and were

approved by the Institutional Animal Care and Use Committees at Boston Children's Hospital (Protocols# 12-02-2146, #14-03-2659R and #15-01-2878R). Mice were genotyped using toe clip (before P8) or ear punch (after P8) and PCR was performed as described previously[26]. For all studies, both male and female mice were used in approximately equal proportions. No randomization paradigm was otherwise applied.

Tissue preparation

Utricle and organ of Corti from *Ush1c c.216G>A* heterozygous or homozygous mutant mice were harvested from postnatal day 0 to 8 (P0 to P8) for electrophysiological studies. Postnatal mouse pups were killed by rapid decapitation. The temporal bones were excised and bathed in MEM (Invitrogen, Carlsbad, CA) supplemented with 10mM HEPES (pH 7.4). The organ of Corti was dissected away without the use of enzyme as described previously[43]. Utricles were removed after 10 min protease treatment (Protease XXIV, Sigma) at 0.1 mg/ml. The excised organs were mounted on round glass coverslips. A pair of thin glass fibers previously glued to the coverslip was placed on the edge of the tissue to stabilize it in a flat position. Tissues were either used acutely or kept in culture in presence of 1% Fetal Bovine Serum. Cultures were maintained for 7 to 10 days and the media was replaced every 2 to 3 days for experiments that involved viral vectors infection *in vitro*.

Scanning electron microscopy (SEM)

SEM was performed at P7, P18 and ~P42 (6 weeks) along the organ of Corti of control and mutant mice. P18 SEM was performed in collaboration with Dr. Edwin Rubel at the University of Washington. Inner ears were fixed in 4% glutaraldehyde in 0.1M sodium phosphate at 4°C overnight. The next day specimens were rinsed three times in 0.1M sodium phosphate buffer (PB) and post-fixed in 1% osmium tetroxide in 0.1M PB for 30 min in an ice bath. Specimens were then rinsed in 0.1M PB and dehydrated through a graded ethanol series: 35%, 70%, 95%, and 100% (x2). Samples were critical point dried, mounted on SEM stubs, and sputter coated with Au/Pd. SEM was performed using a JEOL JSM-840A scanning electron microscope. A similar preparation was performed for P8 and 6 weeks stages by Dr. Géléoc and Dr. Indzhykulian. Organ of Corti explants were fixed in 2.5% glutaraldehyde in 0.1M cacodylate buffer (Electron Microscopy Sciences) supplemented with 2mM $CaCl_2$ for 1h at room temperature. Specimens were dehydrated in a graded series of acetone, critical-point dried from liquid CO_2, sputter-coated with 4–5nm of platinum (Q150T, Quorum Technologies, United Kingdom), and observed with a field emission scanning electron microscope (S-4800, Hitachi, Japan).

Electrophysiological recording

Recordings were performed in standard artificial perilymph solution containing (in mM): 144 NaCl, 0.7 NaH_2PO_4, 5.8 KCl, 1.3 $CaCl_2$, 0.9 $MgCl_2$, 5.6 D-glucose, and 10 HEPES-NaOH, adjusted to pH 7.4 and 320mOsmol/kg. Vitamins (1:50) and amino acids (1:100) were added from concentrates (Invitrogen, Carlsbad, CA). Hair cells were viewed from the apical surface using an upright Axioskop FS microscope (Zeiss, Oberkochen, Germany) equipped with a 63X water immersion objective with differential interference contrast optics. Recording pipettes (3–5 MΩ) were pulled from borosilicate capillary glass (Garner Glass, Claremont, CA) and filled with intracellular solution containing (in mM): 135 KCl, 5

EGTA-KOH, 10 HEPES, 2.5 K_2ATP, 3.5 $MgCl_2$, 0.1 $CaCl_2$, pH 7.4. Currents were recorded under whole-cell voltage-clamp at a holding potential of −64mV at room temperature. Data were acquired using an Axopatch Multiclamp 700A or Axopatch 200A (Molecular devices, Palo Alto, CA) filtered at 10 kHz with a low pass Bessel filter, digitized at ≥20 kHz with a 12-bit acquisition board (Digidata 1322) and pClamp 8.2 and 10.5 (Molecular Devices, Palo Alto, CA). Data were analyzed offline with OriginLab software and are presented as means ± standard deviations unless otherwise noted.

Mechanical stimulation

OHCs and IHCs: Mechanical stimuli were transmitted via a stiff glass probe mounted on a one-dimensional PICMA chip piezo actuator (Physik Instruments, Waldbronn, Gernamy) driven by a 400 mA ENV400 Amplifier (Piezosystem Jena Germany)[44]. The tip of the probe was fired polished (Fire polisher, H602, World Precision Instruments Inc., Sarasota, FL) to fit stereociliary bundle[44]. Deflections were evoked by applying voltage steps filtered with an 8-pole Bessel filter (Khron-Hite, Brockton, MA) at 50 kHz to eliminate residual pipette resonance. Hair bundle deflections were monitored using a C2400 CCD camera (Hamamatsu, Japan). Voltage steps were used to calibrate the motion of the stimulus probe around ± 2μm of its rest position. Video images of the probe were recorded to confirm absence of off-axis motion and calibrate the probe motion (spatial resolution of ~ 4 nm). The 10–90% rise-time of the probe was ~20 μsec. VHCs: Mechanical stimuli were transmitted via a stiff glass probe mounted on a piezoelectric bimorph element. Coupling was performed by gentle suction of the kinocilium into the stimulus pipette. Deflections were evoked by applying voltage steps to the piezoelectrical device which consisted of two bimorphs mounted in series and directly coupled to the stimulus probe. Voltage steps were controlled by pClamp 8.0 software and filtered with a 8 pole Bessel filter at 1 kHz (Khron-Hite, Brockton, MA). Hair bundle deflections were monitored using a C2400 CCD camera (Hamamatsu, Japan). The motion of the stimulus probe was calibrated around (± 2 μm) its rest position prior to the experiments.

Viral vector generation

Harmonin-a1 and harmonin-b1 plasmid were prepared in our laboratory from EGFP tagged labeled constructs graciously provided by Lily Zheng and James Bartles[45] (Department of Cell and Molecular Biology, Northwestern University, Feinberg School of medicine, Chicago, IL). Harmonin-a1 was originally obtained from mouse kidney and harmonin-b1 from isolated mouse cochlea sensory epithelium. We further modified the harmonin-a1 construct to replace the EGFP tag with tdTomato at its N terminal end. Fluorescently labeled and unlabeled constructs were packaged into AAV vectors. Viral vectors were generated by the viral core facility at Boston Children's Hospital and the Gene Transfer Vector Core at the Massachusetts Eye and Ear Infirmary. The following vectors were generated: AAV2/1.CMV.tdTomato::harmonin-a1 4.3×10^13gc/ml (BCH); AAV2/1.CMV.EGFP::harmonin-b1 2.7×10^14 gc/ml (BCH); AAV2/1.CMV.EGFP::harmonin-a1: 2.8×10^12 gc/ml (MEEI); AAV2/Anc80L65.CMV.harmonin-a1: 1.9×10^12 gc/ml (MEEI); AAV2/Anc80L65.CMV.harmonin-b1: 1.7×10^12 gc/ml (MEEI); AAV2/Anc80L65.CMV.tdTomato::harmonin-a1: 4.1×10^12 gc/ml (MEEI); AAV2/Anc80L65.CMV.EGFP::Harmonin-b1: 3.0×10^12 gc/ml (MEEI);

Cloning of the truncated harmonin was performed from total RNA isolated from cochleas of c.216AA mice (RNAqueous micro kit, Ambion) and reverse transcribed with QuantiTect Reverse Transcription kit (Qiagen). The cDNA of trunc-harmonin was amplified by PCR with Platinum Taq DNA polymerase High Fidelity (Invitrogen) and primers:

Trunc-harmonin.F GAGGTACCATGGACCGGAAGGTGGCCCGAG

Trunc-harmomin.RV CAGGATCCGGACAATTTCATCCCCTAC

The 387 bp PCR product was cloned into a shuttle vector with AAV2 inverted terminal repeats (ITRs) where the transgene cassette was driven by a CMV promoter. Custom vector was packaged into the Anc80L65 capsid: AAV2/Anc80L65.CMV.trunc-harm.WPRE: 9.0×10^12 gc/ml (MEEI).

FM1-43 imaging

FM1-43 (Invitrogen) was diluted in extracellular recording solution (5μM) and applied to tissues for 10 seconds and then washed 3 times in extracellular recording solution to remove excess ye and prevent uptake via endocytosis. After 5 minutes the intracellular FM1-43 was imaged using an epifluorescence light source, differential interference contrast optics, and an FM1-43 filter set (Chroma Technologies) on a Zeiss Axioscope FS plus with water immersion 20x, 40x, and 63x objectives. Images were captured at 16-bit with a CCD camera and Argus-20 image processor (Hamamatsu) using background fluorescence subtraction. The same gain and contrast settings were maintained for the acquisition of all images and analyzed offline with Adobe Photoshop or Image-J software.

Confocal imaging

To prepare the tissue for confocal imaging from postnatal mice P0-P8, fixation was performed for 15 min with 4% Paraformaldehyde (PFA). Permeabilization with 0.01% triton and counterstaining with Alexa Fluor phalloidin (Invitrogen, 1/200) was used to labeled actin filaments. Images were obtained on a LSM700 Zeiss confocal microscope. In older mice (4 to 8 weeks), temporal bones were removed after euthanasia and placed in 4% PFA for 1 hour, followed by decalcification for 24 to 36 hours with 120mM EDTA. The sensory epithelium was then dissected out and treated as above for immunostaining. Mouse anti-CTBP2 (BD bioscience #612044, 1/200) or anti-harmonin (Novus Biologicals, LLC #NBP1-89189, 1/100) were applied for 48 hours and incubated with secondary antibody (1/200) and Alexa Fluor Phallodin to label F-actin (1/200) 3–12h at 4°C. Images were acquired on a Zeiss LSM 710 laser confocal microscope (IDDRC Imaging Core grant P30 HD18655) and processed with Zeiss LSM image viewer 4.2.

RT-PCR

cDNA was prepared from 6 auditory organs of P2-P3 wild-type, heterozygous and homozygous *Ush1c c.216G>A* mice using QuantiTect Revese Transcription Kit (Qiagen). cDNA encoding full length (450bp) or truncated harmonin (−35bp) was amplified using the following primers: Forward primer mUsh1c_Ex2F: 5′ CTCATTGAAAATGACGCAGAGAAGG 3′, Reverse mUsh1c_Ex5R: 5′ TCTCACTTTGATGGACACGGTCTT 3′. These primers are specific for mouse *Ush1c*

sequences and will amplify both endogenous and AAV2-derived *Ush1c* as the target sequence is outside the region of the human knocked in portion of the *Ush1c* c.216A allele. DNA and RNA levels were also assessed from mouse tissue collected at six weeks post-treatment. DNA and RNA were isolated from the cochlea using TRIzol reagent (Life Technologies, Carlsbad, CA) according to the manufacturer's protocol. RNA was reverse transcribed using GoScript reverse transcription system (Promega, Madison, WI). Radiolabeled PCR was carried out using GoTaq Green Master Mix (Promega, Madison, WI). For viral DNA amplification, primers specific for mouse *Ush1c*: mUsh1c_Ex3F (5′-GAACCCAACCGCCTGCCG) and mUsh1c_Ex4WTR (5′-TGCAGACGGTCCAAGCGT-3′) were used. These primers only amplify the viral *Ush1c* DNA because the homozygous *Ush1c*.216AA mice have the human *USH1C* c.216A gene knocked-in at exons 3 and 4, replacing the mouse sequence (32). For cDNA amplification of full-length (450bp) and aberrantly spliced/truncated harmonin (415bp), the same primers as above were used (mUsh1c_Ex2F and mUsh1c_Ex5R). Gapdh primers were: mGapdh_Ex3F (5′-GTGAGGCCGGTGCTGAGTATG-3′) and mGapdh_Ex4R (5′-GCCAAAGTTGTCATGGATGAC-3′). Products were separated on a 6% nondenaturing polyacrylamide gel and quantified using a Typhoon 9400 phosphorimager (GE Healthcare).

Round window membrane (RWM) injection

RWM injections were performed as approved by the Institutional Animal Care and Use Committees at Boston Children's Hospital animal protocol #15-01-2878R. 0.8 μl-1ul of AAV vectors were injected in neonatal mice P0-P1 and P10-P12. P0-P1 mice were first anesthetized using hypothermia exposure while P10-P12 mice were anesthetized with isoflurane. Upon anesthesia, post-auricular incision was made to expose the otic bulla and visualize the cochlea. Injections were done through the RWM with a glass micropipette controlled by a micromanipulator[6]. The volume of the injected materials was controlled at an approximately 0.02 μl/min for 10 min. Standard post-operative care was applied. Sample size for *in vivo* studies were determined on a continuing basis to optimize the sample size and decrease the variance.

Auditory brainstem responses (ABRs) and distortion products (DPOAEs)

ABRs and DPOAEs were recorded from mice anesthetized with xylazine (5–10mg/kg i.p.) and ketamine (60 – 100mg/kg i.p.). Subcutaneous needle electrodes were inserted into the skin a) dorsally between the two ears (reference electrode); b) behind the left pinna (recording electrode); and c) dorsally at the rump of the animal (ground electrode). The meatus at the base of the pinna was trimmed away to expose the ear canal. For ABR recordings the ear canal and hearing apparatus (EPL Acoustic system, MEEI, Boston) were presented with 5-millisec tone pips. The responses were amplified (10,000 times), filtered (0.1–3 kHz), and averaged with an analog-to-digital board in a PC based data-acquisition system (EPL, Cochlear function test suite, MEEI, Boston). Sound level was raised in 5 to 10 dB steps from 0 to 110 dB sound pressure level (decibels SPL). At each level, 512 to 1024 responses were averaged (with stimulus polarity alternated) after "artifact rejection". Threshold was determined by visual inspection. Data were analyzed and plotted using Origin-2015 (OriginLab Corporation, MA). Thresholds averages ± standard deviations are presented unless otherwise stated. For DPOAEs, f1 and f2 primary tones (f2/f1 = 1.2) were

presented with f2 varied between 5.6 and 45.2 kHz in half-octave steps and L1–L2 = 10 dB SPL. At each f2, L2 was varied between 10 and 80 dB in 10dB increments. DPOAE threshold was defined from the average spectra as the L2-level eliciting a DPOAE of magnitude 5 dB above the noise floor. The mean noise floor level was under 0 dB across all frequencies. Stimuli were generated with 24-bit digital I–O cards (National Instruments PXI-4461) in a PXI-1042Q chassis, amplified by an SA-1 speaker driver (Tucker–Davis Technologies, Inc.), and delivered from two electrostatic drivers (CUI CDMG15008-03A) in our custom acoustic system. An electret microphone (Knowles FG-23329-P07) at the end of a small probe tube was used to monitor ear-canal sound pressure. The majority of these experiments were not performed under blind conditions.

Acoustic startle responses

The acoustic startle responses (ASR) were measured using the Startle Monitor (Kinder Scientific). Mice were placed in a small-sized, nonrestrictive, cubical Plexiglas recording chamber (27 cm × 10 cm × 12.5 cm) fixed on a piezo/plexiglass sensing assembly and allowed to acclimate for 5 min with a 60 dB background white noise. Each session consisted of 35 trials, during which a single noise pulse ranging in 10 dB intensities from 60–120 dB was delivered with an inter-trial interval averaging 30s (25–35 s range). Pulses were arranged in a pseudorandom order, on a constant 60 dB back ground noise to limit external noise interference. The Startle Monitor system reduced the response to each pulse into measurements of first N, max N, and max time of the response (ms), for calculations of peak startle response (ASR amplitude) and time from stimulus to peak startle response (ASR latency). ASR were all conducted blind.

Vestibular assessment

Vestibular function was assessed using open field and rotarod balance test. The open field test was conducted using a circular frame measuring 42cm in diameter, placed inside a sound chamber with overhead LED lighting, set to 30lux at the center, inside a dimmed room. Mice were placed one at a time inside the circular open field, and allowed to explore for 5min. Behavior was recorded and tracked using Ethovision XT, enabling measures of distance traveled and velocity. Open field assessments were all conducted blind. The rotarod performance involved placement of mice on a rod in an enclosed housing that began rotating at 4 rpm and accelerated at a rate of 0.1 rpm s^{-1}. The mice were placed on the rods on day one for 5 min to get familiarized with the equipment. The next day, the animals were placed on the rods for a total of 5 trials. A 5 min resting period was imposed between trials. The length of time the animals were able to remain on the device before dropping onto the instrumented floor of the housing was displayed on a timer and recorded after each test run.

Statistical analyses

Test and control vectors were evaluated in at least three mice per group at each time point to ensure reproducibility. Sample sizes are noted in figure legends. All animals with successful RWM injection were included in the study analysis. Those animals with unsuccessful injection were excluded from the mean but included in the legend for full disclosure. Injection success was determined according to ABR recovery with thresholds < 80 dB SPL. Statistical analyses were performed with Origin 2016 (OriginLab Corporation). Data are

presented as means ± standard deviations (S.D) or standard error of the mean (S.E.M.) as noted in the text and figure legend. One-way analysis of variance (ANOVA) or Student t-test was used to determine significant differences between the means. In the box plot graphs, the ends of whisker is defined by maximum and minimum values. Central rectangle spans from first quartile to third quartile. The segment in the rectangle indicates median and the square dot indicates the mean.

Supplementary Material

Refer to Web version on PubMed Central for supplementary material.

Acknowledgments

This work was supported by the Manton Center for Orphan Disease Pilot Award 2011 to G. Geleoc (Boston Children's Hospital), the Bertarelli Foundation, Program in Translational Neuroscience and Neuroengineering, Kidz-b-Kidz Foundation (now Arts for USH), the Jeff and Kimberly Barber Gene Therapy Research Fund and a consortium agreement under a primary award from the Foundation Fighting Blindness, Cost Center #7 5794 (P.I. L. Vandenberghe). A. Indzhykulian received support from R01DC000304 (DP Corey). S. Heman-Ackah was the recipient of the diversity faculty fellowship award from Harvard Medical School. Behavior and Viral Cores at Boston Children's Hospital are supported by the Boston Children's Hospital Intellectual and Developmental Disabilities Research Center (BCH IDDRC), P30 HD18655. M. Hasting contribution was supported by R01DC012596. We thank M. Valero (EPL, MEEI) for assistance with ABRs, S. Xu (BCH core) for help with the behavior work, C. Wang (BCH viral core) for AAV production, and C. Nist-Lund (BCH) for technical assistance.

References

1. Chien WW, et al. Gene Therapy Restores Hair Cell Stereocilia Morphology in Inner Ears of Deaf Whirler Mice. Mol Ther. 2016; 24:17–25. [PubMed: 26307667]
2. Askew C, et al. Tmc gene therapy restores auditory function in deaf mice. Sci Transl Med. 2015; 7:295ra108.
3. Akil O, et al. Restoration of hearing in the VGLUT3 knockout mouse using virally mediated gene therapy. Neuron. 2012; 75:283–293. [PubMed: 22841313]
4. Boughman JA, Vernon M, Shaver KA. Usher syndrome: definition and estimate of prevalence from two high-risk populations. J Chronic Dis. 1983; 36:595–603. [PubMed: 6885960]
5. Smith RJ, et al. Clinical diagnosis of the Usher syndromes. Usher Syndrome Consortium. Am J Med Genet. 1994; 50:32–38. [PubMed: 8160750]
6. Vernon M. Usher's syndrome — deafness and progressive blindness. Clinical cases, prevention, theory and literature survey. J Chronic Dis. 1969; 22:133–151. [PubMed: 4897966]
7. Weil D, et al. Defective myosin VIIA gene responsible for Usher syndrome type 1B. Nature. 1995; 374:60–61. [PubMed: 7870171]
8. Weston MD, et al. Myosin VIIA mutation screening in 189 Usher syndrome type 1 patients. Am J Hum Genet. 1996; 59:1074–1083. [PubMed: 8900236]
9. Adato A, et al. Mutation profile of all 49 exons of the human myosin VIIA gene, and haplotype analysis, in Usher 1B families from diverse origins. Am J Hum Genet. 1997; 61:813–821. [PubMed: 9382091]
10. Liu XZ, Newton VE, Steel KP, Brown SD. Identification of a new mutation of the myosin VII head region in Usher syndrome type 1. Hum Mutat. 1997; 10:168–170. [PubMed: 9259201]
11. Bitner-Glindzicz M, et al. A recessive contiguous gene deletion causing infantile hyperinsulinism, enteropathy and deafness identifies the Usher type 1C gene. Nat Genet. 2000; 26:56–60. [PubMed: 10973248]
12. Verpy E, et al. A defect in harmonin, a PDZ domain-containing protein expressed in the inner ear sensory hair cells, underlies Usher syndrome type 1C. Nat Genet. 2000; 26:51–55. [PubMed: 10973247]

13. Bolz H, et al. Mutation of CDH23, encoding a new member of the cadherin gene family, causes Usher syndrome type 1D. Nat Genet. 2001; 27:108–112. [PubMed: 11138009]
14. Bork JM, et al. Usher syndrome 1D and nonsyndromic autosomal recessive deafness DFNB12 are caused by allelic mutations of the novel cadherin-like gene CDH23. Am J Hum Genet. 2001; 68:26–37. [PubMed: 11090341]
15. Ahmed ZM, et al. Mutations of the protocadherin gene PCDH15 cause Usher syndrome type 1F. Am J Hum Genet. 2001; 69:25–34. [PubMed: 11398101]
16. Alagramam KN, et al. The mouse Ames waltzer hearing-loss mutant is caused by mutation of Pcdh15, a novel protocadherin gene. Nat Genet. 2001a; 27:99–102. [PubMed: 11138007]
17. Alagramam KN, et al. Mutations in the novel protocadherin PCDH15 cause Usher syndrome type 1F. Hum Mol Genet. 2001b; 10:1709–1718. [PubMed: 11487575]
18. Weil D, et al. Usher syndrome type I G (USH1G) is caused by mutations in the gene encoding SANS, a protein that associates with the USH1C protein, harmonin. Hum Mol Genet. 2003; 12:463–471. [PubMed: 12588794]
19. Riazuddin S, et al. Alterations of the CIB2 calcium- and integrin-binding protein cause Usher syndrome type 1J and nonsyndromic deafness DFNB48. Nat Genet. 2012; 44:1265–1271. [PubMed: 23023331]
20. Boeda B, et al. Myosin VIIa, harmonin and cadherin 23, three Usher I gene products that cooperate to shape the sensory hair cell bundle. EMBO J. 2002; 21:6689–6699. [PubMed: 12485990]
21. Lefevre G, et al. A core cochlear phenotype in USH1 mouse mutants implicates fibrous links of the hair bundle in its cohesion, orientation and differential growth. Development. 2008; 135:1427–1437. [PubMed: 18339676]
22. Grillet N, et al. Harmonin mutations cause mechanotransduction defects in cochlear hair cells. Neuron. 2009; 62:375–387. [PubMed: 19447093]
23. Michalski N, et al. Harmonin-b, an actin-binding scaffold protein, is involved in the adaptation of mechanoelectrical transduction by sensory hair cells. Pflugers Arch. 2009; 459:115–130. [PubMed: 19756723]
24. Gregory FD, et al. Harmonin inhibits presynaptic Cav1.3 Ca(2)(+) channels in mouse inner hair cells. Nat Neurosci. 2011; 14:1109–1111. [PubMed: 21822269]
25. Gregory FD, Pangrsic T, Calin-Jageman IE, Moser T, Lee A. Harmonin enhances voltage-dependent facilitation of Cav1.3 channels and synchronous exocytosis in mouse inner hair cells. J Physiol. 2013; 591:3253–3269. [PubMed: 23613530]
26. Lentz J, Pan F, Ng SS, Deininger P, Keats B. *Ush1c216A* knock-in mouse survives Katrina. Mutat Res. 2007; 616:139–144. [PubMed: 17174357]
27. Lentz J, et al. The USH1C 216G-->A splice-site mutation results in a 35-base-pair deletion. Hum Genet. 2005; 116:225–227. [PubMed: 15578223]
28. Lentz JJ, et al. Deafness and retinal degeneration in a novel USH1C knock-in mouse model. Dev Neurobiol. 2010; 70:253–267. [PubMed: 20095043]
29. Landegger L, et al. A synthetic AAV vector enables safe and efficient gene transfer to the mammalian inner ear. Nat Biotechnol. 2017; 35:XX–XX.
30. Lentz JJ, et al. Rescue of hearing and vestibular function by antisense oligonucleotides in a mouse model of human deafness. Nat Med. 2013; 19:345–350. [PubMed: 23380860]
31. Gale JE, Marcotti W, Kennedy HJ, Kros CJ, Richardson GP. FM1-43 dye behaves as a permeant blocker of the hair-cell mechanotransducer channel. J Neurosci. 2001; 21:7013–7025. [PubMed: 11549711]
32. Meyers JR, et al. Lighting up the senses: FM1-43 loading of sensory cells through nonselective ion channels. J Neurosci. 2003; 23:4054–4065. [PubMed: 12764092]
33. Geleoc GS, Holt JR. Developmental acquisition of sensory transduction in hair cells of the mouse inner ear. Nat Neurosci. 2003; 6:1019–1020. [PubMed: 12973354]
34. Zinn E, et al. In Silico Reconstruction of the Viral Evolutionary Lineage Yields a Potent Gene Therapy Vector. Cell Rep. 2015; 12:1056–1068. [PubMed: 26235624]
35. Kho ST, Pettis RM, Mhatre AN, Lalwani AK. Safety of adeno-associated virus as cochlear gene transfer vector: analysis of distant spread beyond injected cochleae. Mol Ther. 2000; 4:368–373.

36. Bedrosian JC, et al. *In vivo* delivery of recombinant viruses to the fetal murine cochlea: transduction characteristics and long-term effects on auditory function. Mol Ther. 2006; 14:328–335. [PubMed: 16765094]

37. Wang L, Jiang H, Brigande JV. Gene transfer to the developing mouse inner ear by *in vivo* electroporation. J Vis Exp. 2012; 64 pii: 3653.

38. Depreux FF, et al. Antisense oligonucleotides delivered to the amniotic cavity in utero modulate gene expression in the postnatal mouse. Nucleic Acids Res. 2016; 44:9519–9529. [PubMed: 27683224]

39. Clark KR, Sferra TJ, Johnson PR. Recombinant adeno-associated viral vectors mediate long-term transgene expression in muscle. Hum Gene Ther. 1997; 8:659–669. [PubMed: 9113506]

40. Duan D, et al. Circular intermediates of recombinant adeno-associated virus have defined structural characteristics responsible for long-term episomal persistence in muscle tissue. J Virol. 1998; 72:8568–8577. [PubMed: 9765395]

41. Noben-Trauth K, Zheng QY, Johnson KR. Association of cadherin 23 with polygenic inheritance and genetic modification of sensorineural hearing loss. Nat Genet. 2000; 35:21–23.

42. Kane KL, et al. Genetic background effects on age-related hearing loss associated with Cdh23 variants in mice. Hear Res. 2012; 283:80–88. [PubMed: 22138310]

43. Lelli A, Asai Y, Forge A, Holt JR, Geleoc GS. Tonotopic gradient in the developmental acquisition of sensory transduction in outer hair cells of the mouse cochlea. J Neurophysiol. 2009; 101:2961–2973. [PubMed: 19339464]

44. Stauffer EA, Holt JR. Sensory transduction and adaptation in inner and outer hair cells of the mouse auditory system. J Neurophysiol. 2007; 98:3360–3369. [PubMed: 17942617]

45. Zheng L, Zheng J, Whitlon DS, Garcia-Anoveros J, Bartles JR. Targeting of the hair cell proteins cadherin 23, harmonin, myosin XVa, espin, and prestin in an epithelial cell model. J Neurosci. 2010; 30:7187–7201. [PubMed: 20505086]

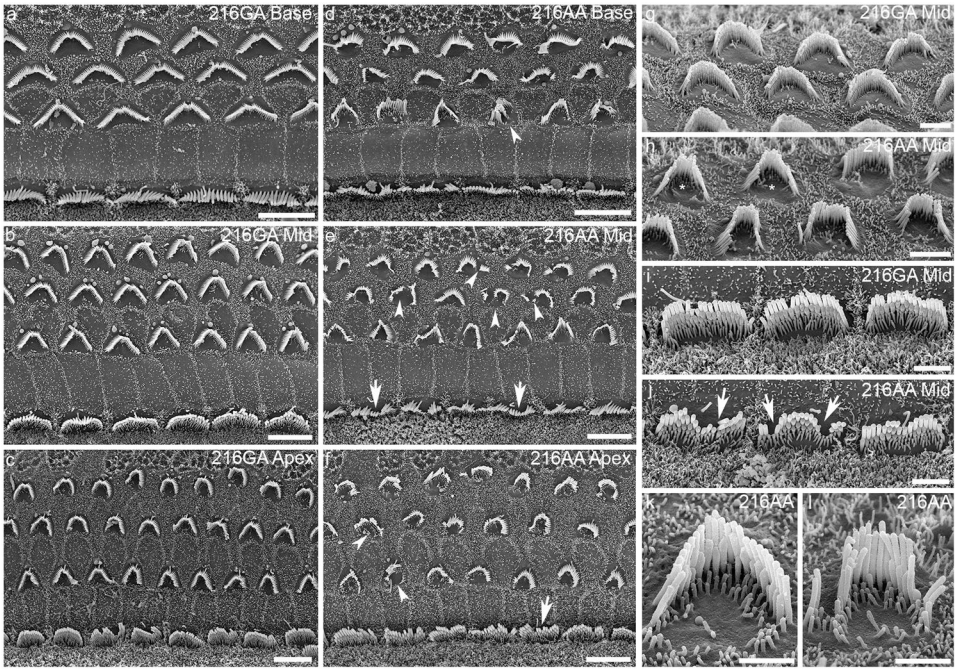

Figure 1. Scanning electron microscopy of the organ of Corti in *Ush1c c.216G>A* mice at P8

(a–f) Basal, middle and apical regions of the organ of Corti were imaged in P8 c.216GA (n = 3 mice) and c.216AA (n = 4 mice) mice. OHC and IHC hair bundles were preserved in heterozygous mice but some hair bundles appeared disorganized along the organ of Corti in homozygous 216AA mice. (g–l) High magnification images revealed fragmented and disorganized bundles with disruptions in the staircase array in many but not all OHC (g–h) and IHCs (i–j). Examples of OHC hair bundles imaged in the middle region of the organ at P8 illustrate a preserved (k) and a disorganized hair bundle (l) present in the same preparation. Stars indicate preserved hair bundles; arrowhead, disorganized hair bundles; and arrows, wavy IHC bundles. Scale bars low mag.: 5 μm (a–f); high mag.: 2 μm (g), 3 μm (h), 2 μm (i–j) and 1 μm (k,l).

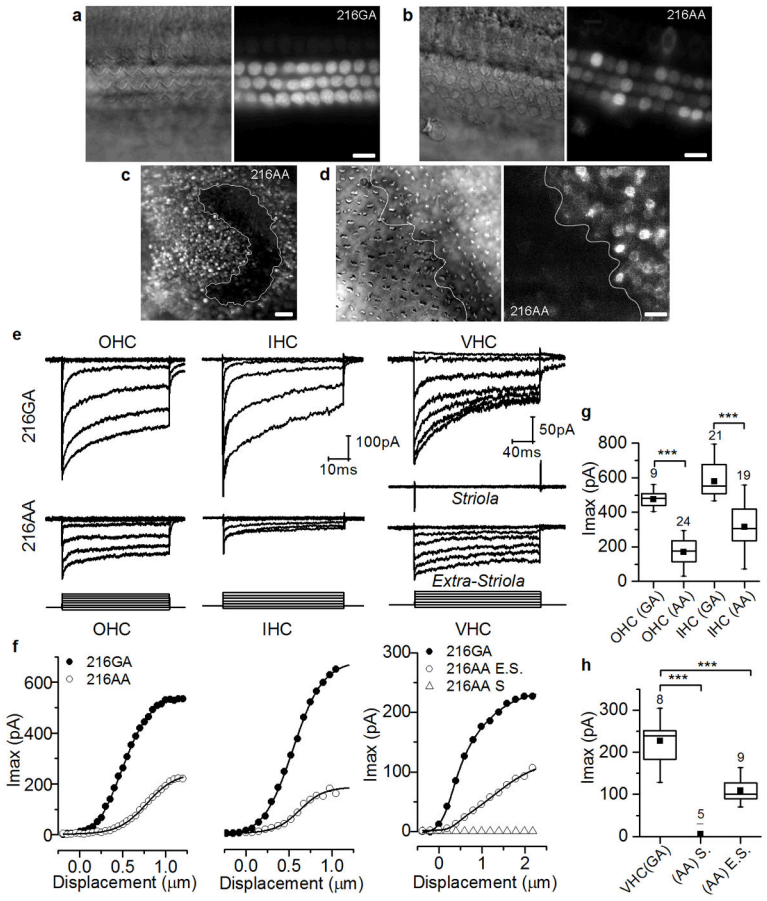

Figure 2. Mechanotransduction in hair cells of *Ush1c c.216G>A* neonatal mice

(a–d) The permeable styryl dye FM1-43 was used to assess the presence of open transduction channels in hair cells of c.216GA and c.216AA mice. In the organ of Corti, FM uptake was reduced in sensory hair cells of c.216AA mice at P4 (a–b, mid base). Note that IHC FM1-43 fluorescence appears dimmer as IHCs are in a different focal plane. Left: DIC, Right: FM1-43; Scale bar 10μm. In the utricle, FM1-43 uptake was restricted to the extra-striola region in c.216AA mutants at P6 (c; scale bar 50μm) while utricular hair cells retained gross normal bundle morphology as assessed by DIC (d; scale bar 10μm). The white lines on panel c and d delineate the striola (no uptake) and extra-striola regions (uptake). Experiment was repeated three times. (e–h) Mechanotransduction was assessed in OHCs, IHCs and VHCs in neonatal c.216GA and c.216AA mice (number of mice recorded from respectively are: n= 7, 6 for OHCs, n= 2, 4 for IHCs and n= 2, 6 for VHCs, number of cells are indicated above the bar graph; Holding potential: −60mV). Representative transduction currents (e), their associated current/displacement plots fitted with a second order Boltzmann function (f) and average peak transduction current are plotted (g–h). In the cochlea, recordings were obtained in the middle and mid-apical turn of the organ at P3-P6. In the utricle transduction currents were recorded from VHCs of the extra-striola (E.S.) and striola (S.) region between P5 and P7 (e–f). While hair bundles appeared well preserved under DIC, smaller average transduction currents were evoked in c.216AA mutants (h).

Average peak transduction was significantly different between the two genotypes in OHCs, IHCs and VHCs (***P < 0.01, One-way ANOVA).

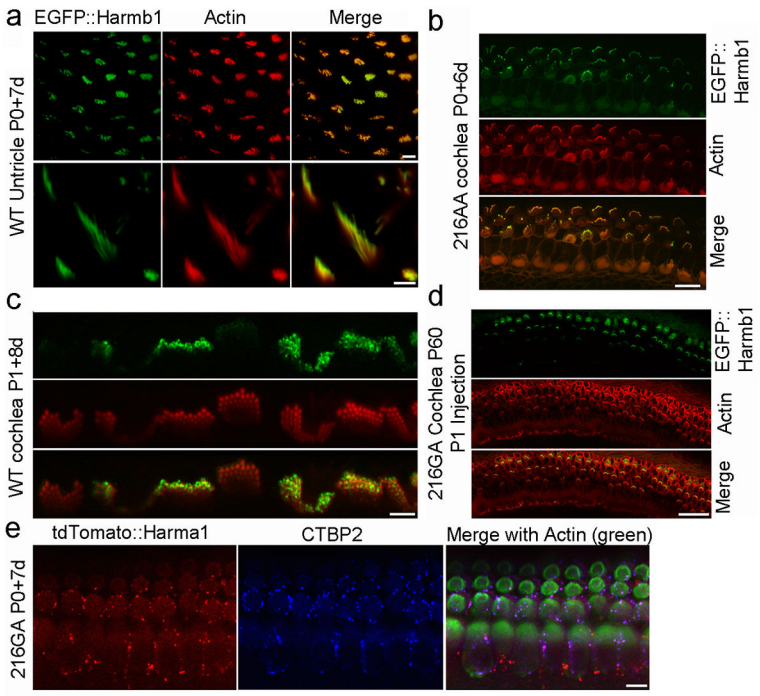

Figure 3. Expression and localization of fluorescently labeled harmonin in tissues exposed to adeno-associated viral vectors *in vitro* and *in vivo*

(a–c) Acutely dissected P0-P1 inner ear tissue were exposed to AAV2/1 vectors for 24h, kept in culture for 7 to 8 days before being fixed, counterstained (Alexa Fluor phalloidin, Invitrogen) and imaged with a Zeiss LSM confocal microscope. A large number of sensory hair cells were infected in wild-type utricle and expression of harmonin-b1 fused to EGFP was evident in most hair cells with specific localization at the apex of the sensory hair bundle (a, scale bar: 10 μm- upper panels; 5μm- lower panels). Similarly expression of EGFP::harmonin-b1 was evident at the tip of the stereocilia in OHCs and IHCs of c.216AA and wild-type mice (b, scale bar: 10 μm; c, scale bar: 3μm). When 1 μl AAV2/1.CMV.EGFP::harmonin-b1 vectors were injected at P1, EGFP signal was detected in some IHCs and OHCs at P60 in the left injected ear (d, scale bar: 30 μm). Exogenous tdTomato::harmonin-a1 was detected in the cell body of IHCs and OHCs in P7 organotypic cultures exposed to AAV2/1.CMV.tdTomato::harmonin-a1 for 24 h at P0 (e, scale bar: 5μm). Some harmonin-a1 puncta were colocalized with CTBP2 (blue; mouse anti-CTBP2 1/200, BD bioscience) in particular at the base of the sensory cells presumably near the ribbon synapse (arrowheads). No expression was observed in the stereociliary bundle.

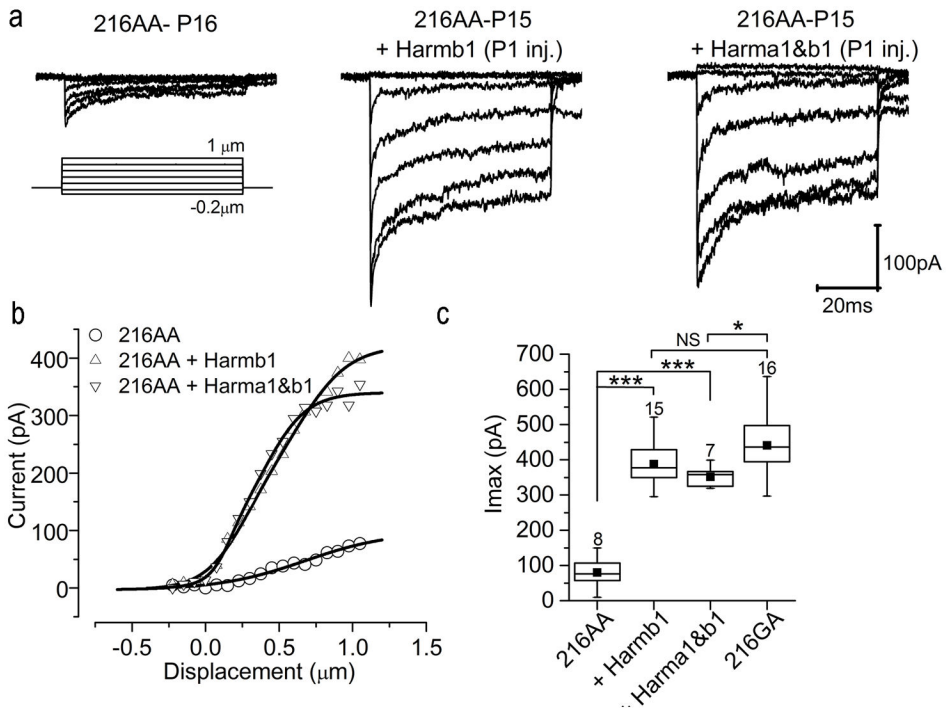

Figure 4. Recovery of mechanotransduction in hair cells of mice injected with Anc80L65 harmonin vectors

(a–c) Mechanotransduction currents were recorded in IHCs of c.216AA uninjected control mice (n=8 cells, one mouse) and c.216AA mice injected at P1 with AAV2/Anc80L65.CMV.harmonin-b1 (0.8 μl, 1.9×10^12 gc/ml, n=15 cells, one mouse) or a combined injection of the AAV2/Anc80L65.CMV.harmonin-a1 (1.7×10^12 gc/ml) and AAV2/Anc80L65.CMV.harmonin-b1 (0.5 μl + 0.5 μl, n=7 cells, one mouse). Tissue was extracted at P5-P6, before the cochlea became ossified, and was maintained in culture for 10 days. (9 to 10 DIV). While small mechanotransduction currents could be induced by hair bundle stimulations of c.216AA mice, larger currents were evoked in c.216AA mice injected with vectors driving harmonin-b1 or dual harmonin-a1 and -b1 expression (a). Corresponding I/X curve for each dataset and double Boltzmann fitting function. Respective maximal mechanotransduction current Imax= 102.1 pA (c.216AA); 424.3 pA (c.216AA + harmonin-b1) and 341.1 pA (c.216AA + harmonin-a1&-b1) (b). Average responses (Mean ± S.D.) show significant recovery of transduction (***P < 0.001) for harmonin-b1 and harmonin-a1 +-b1 injected relative to uninjected mice. Average transduction currents were not significantly different in harmonin-b1 injected mice and c.216GA control mice (N.S. P>0.5). Recovery of mechanotransduction was also not significantly improved when harmonin-a and harmonin-b were combined. (c), one-way ANOVA.

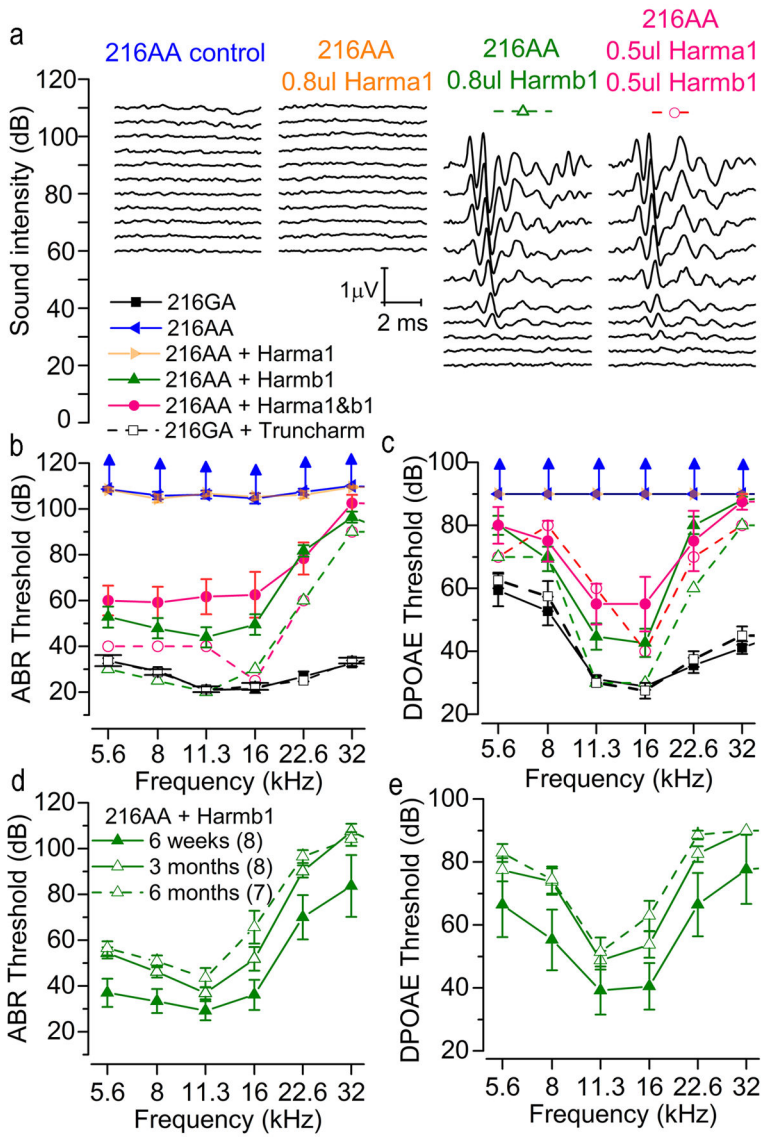

Figure 5. ABR and DPOAE threshold recovery in mice injected at P1 with AAV2/ Anc80L65.CMV.harmonin-b1

(a) Representative ABR responses for 16 kHz tones in 6 weeks old c.216AA control mice and c.216AA mice injected at P1 via RWM injection of vectors encoding harmonin-a1(0.8 μl, 1.7×10^12 gc/ml), harmonin-b1 (0.8 μl, 1.9×10^12 gc/ml) or a combination of the two (0.5 μl + 0.5 μl). Recovered ABR thresholds near 30 dB were measured in mice injected with harmonin-b1 alone or harmonin-a1 and b1 together. (b) Mean ABR responses obtained for: c.216 AA (n=13); c.216GA (n=12); c.216GA + trunc-harmonin (n=4); c.216AA + harmonin-a1 (n=12); c.216AA + harmonin-b1 (n=19 with rescued ABR thresholds < 80 dB of 25 tested); c.216AA + harmonin-a1&-b1 (n=6 rescued with ABR thresholds <80 dB/11 tested). Mean ± S.E, continuous lines. Dotted lines: ABR thresholds for the entire frequency range in mice whose 16 kHz recordings are shown in panel a. (c) Mean DPOAEs responses obtained for: c.216AA (n=13); c.216GA (n=12); c.216GA + trunc-harmonin (n=4); c. 216AA + harmonin-a1 (n=12); c.216AA + harmonin-b1 (n=15 rescued with DPOAE

thresholds <70 dB/25 tested); c.216AA + harmonin-a1&-b1 (n=4 rescued with DPOAEs <70 dB/11 tested). Mean ± S.E, continuous lines. Dotted lines: DPOAEs thresholds for the four mice whose recordings are illustrated in panel A. Arrows indicate that the thresholds are higher than the maximal stimulus level tested. (d–e) ABRs and DPOAEs responses obtained at 6 weeks and 3 months in eight mice that showed initial ABR thresholds under or equal to 45 dB SPL. Seven of the eight mice were kept for 6 months (one taken for histology) and had ABRs and DPOAEs assessed (dotted line). Mean ± S.E. While ABRs and DPOAEs thresholds shifts were evident over the first three month, hearing rescue was still prominent at 6 months of age in the lower frequency range.

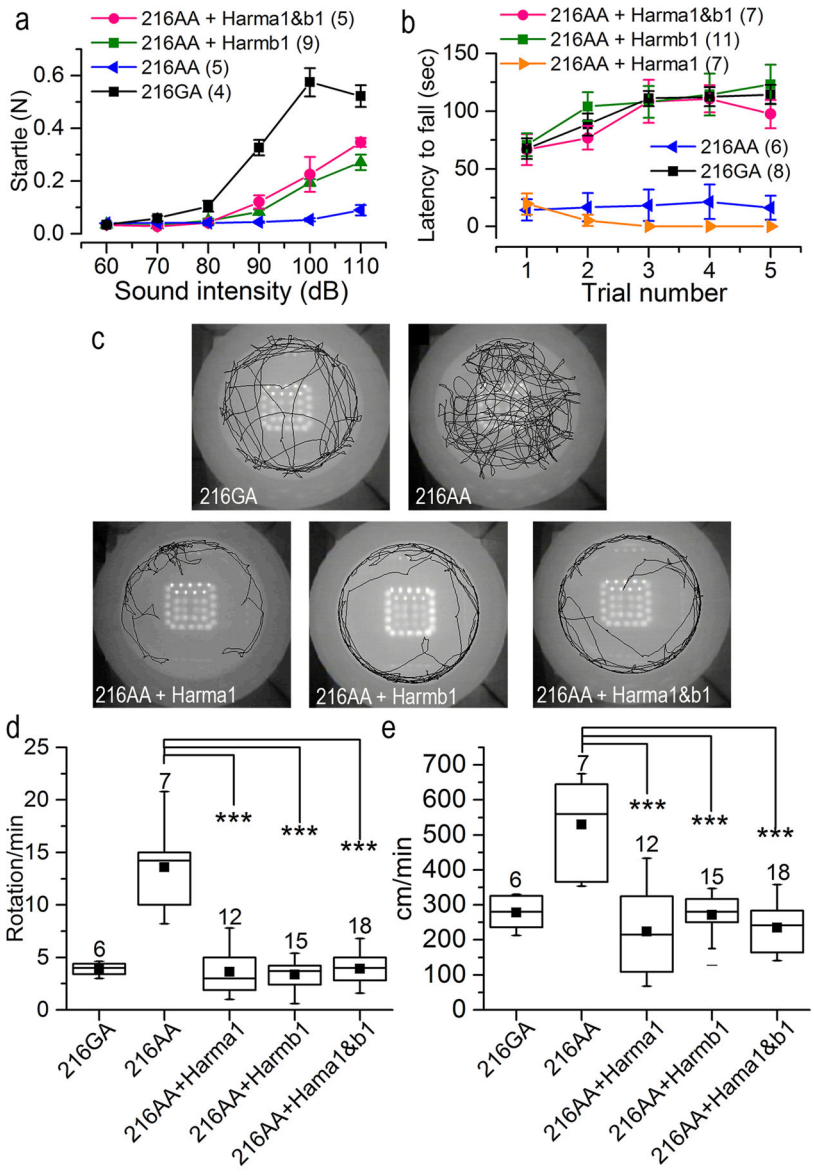

Figure 6. Startle response, rotarod performance and open field behavior recovery in mice injected at P1 with AAV2/Anc80L65.CMV.harmonin-a1 and AAV2/Anc80L65.CMV.harmonin-b1

(a) Startle response to white noise stimuli was recorded in 6 weeks old control c.216GA, c. 216AA mice and injected mice. Partial but significant startle rescue was evident in mice injected with harmonin-b1 but not harmonin-a1 (data overlap with control c.216AA mice). Averages ± S.E. are shown for all mice tested. Statistical analysis: 216AA relative to 216AA + Harm a1&b1: p=0.008 at 100db; p= 0.005 at 110dB; 216AA relative to 216AA + Harm b1: p= 0.007 at 100dB; 0.001 at 110dB, Student t-test. (b) Rotarod performance was recorded between 4 and 6 weeks in control c.216GA, c.216AA and injected mice. Full recovery was observed in all mice tested that were injected with harmonin-b1 and harmonin-a1/b1. No recovery was observed for harmonin-a1 alone. Averages ± S.E. are shown for all mice tested. (c–e) Open field observations were performed in 42 cm wide arena for 5 min in

6 weeks old control c.216GA, c.216AA and injected mice. Representative tracks over 2.5 min are shown (c). While c.216AA mice explore the entire field, and perform repetitive full-body rotations, c.216AA mice injected at P1 with harmonin-a1, harmonin-b1 or the combination of the two vectors demonstrate normal behavior similar to their heterozygous c.216GA. Mean ± S.D. for the number of rotations (d) and distance covered (e) per minute for all mice tested. Significant recovery ***$P < 0.001$ was observed between the uninjected and injected mice. Statistical analysis by one-way ANOVA.

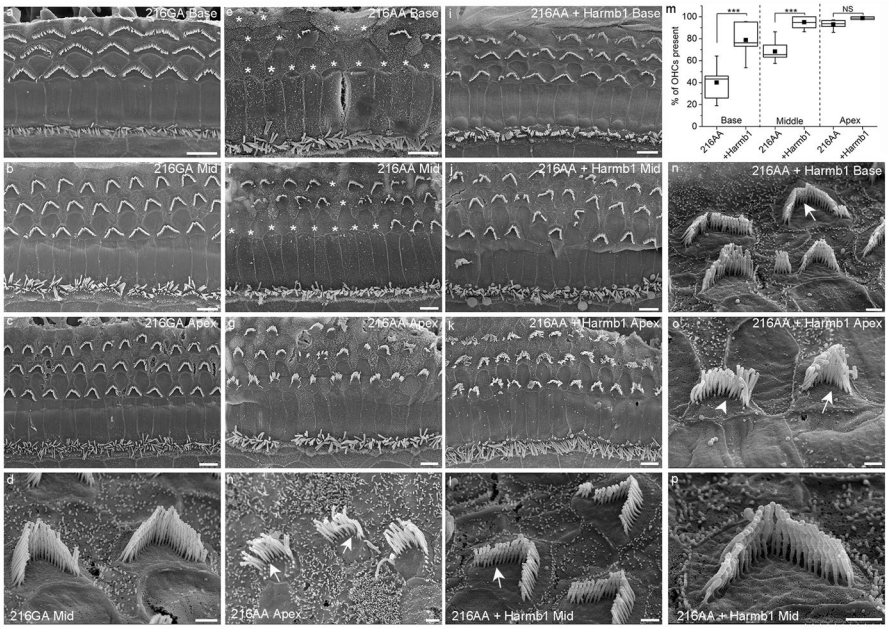

Figure 7. Scanning electron microscopy of the organ of Corti in mice injected with AAV2/Anc80L65.CMV.harmonin-b1

Basal, Middle and Apical regions of the organ of Corti were imaged at six weeks in c.216GA (a–d), c.216AA (e–h) and c.216AA (i–l, n–p) mice injected at P1 (RMW injection 0.8 μl AAV2/Anc80L65.CMV.harmonin-b1). OHC and IHC hair bundles were preserved in c.216GA mice but appeared disorganized along the organ of Corti in c.216AA mice. Noticeable hair cell loss (asterisk) and hair bundle disorganization was observed in c.216AA mice with more pronounced degeneration in the basal end of the organ. Hair bundles of c.216AA mice lacked normal stereocilia rows. The shorter rows appeared to be retracted while the tallest rows were maintained in c.216AA mice (arrow). While hair cell loss and bundle disorganization were still evident in rescued c.216AA mice, hair cell survival was noticeably higher in the basal and middle regions of the Organ. Hair cell counts are summarized in the bar graph. A total of 1824 cells were counted in c.216AA mice (4 ears) and 792 in rescued c.216AA mice (2 ears). Mean ± S.E. High magnification imaging reveals rescue of the staircase array in injected c.216AA mice (arrow) in many but not all cells (arrowhead). Scale bar low magnification: 5 μm; high magnification: 1 μm.